MHD Equilibrium and Stability of Tokamaks and RFP Systems with 3D Helical Cores

W. A. Cooper

Ecole Polytechnique Fédérale de Lausanne, Association EURATOM-Confédération Suisse, Centre de Recherches en Physique des Plasmas, CH1015 Lausanne, Switzerland.

Collaborators

EPFL/CRPP: J. P. Graves, O. Sauter, A. Pochelon, L. Villard
Consorzio RFX: D. Terranova, M. Gobbin, P. Martin, L. Marrelli, I. Predebon
ORNL: S. P. Hirshman
Culham Science Centre: I. T. Chapman

MOTIVATION

Manifestation of internal 3D structures in axisymmetric devices:

- SHAx states in RFX-mod
  - –R. Lorenzini et al., Nature Physics **5** (2009) 570
- "Snakes" in JET
  - –A. Weller et al., Phys. Rev. Lett. **59** (1987) 2303
- Disappearance of sawteeth but continuous dominantly $n = 1$ mode in TCV at high elongation and current
  - –H. Reimerdes et al., Plasma Phys. Control. Fusion **48** (2006) 1621
  - –Y. Camenen et al., Nucl. Fusion **47** (2007) 586
- Change of sawteeth from kink-like to quasi-interchange-like with plasma shaping in DIII-D
  - –E. A. Lazarus et al., Plasma Phys. Contr. Fusion **48** (2006) L65
- Long-lived saturated modes in MAST
  - –I. T. Chapman et al., Nucl. Fusion **50** (2010) 045997

THEORY REVIEW

- Analytic studies of ideal nonlinearly saturated $m = 1, n = 1$ modes
  - –Avinash, R.J. Hastie, J.B. Taylor, Phys. Rev. Lett. **59** (1987) 2647
  - –M.N. Bussac, R. Pellat, Phys. Rev. Lett. **59** (1987) 2650
  - –F.L. Waelbroeck, Phys. Fluids **B 59** (1989) 499
- Pellet deposition in magnetic island on $q = 1$ surface
  - –J.A. Wesson, Plasma Phys. Control. Fusion **B 37** (1995) A337
- Large scale simulations of nonlinearly saturated MHD instability
  - –L.A. Charlton et al., Phys. Fluids **B 59** (1989) 798
  - –H. Lütjens, J.F. Luciani, J. Comput. Phys. **227** (2008) 6944
- Bifurcated equilibria due to ballooning modes with the NSTAB code
  - –P. Garabedian, Proc. Natl. Acad. Sci. USA **103** (2006) 19232
- RFX-mod SHAx MHD equilibria
  - –D. Terranova et al., in Plasma Phys. Contr. Fusion **52** (2010)
- Bifurcated tokamak equilibria similar to a saturated internal kink
  - –W.A. Cooper et al., Phys. Rev. Lett. **105** (2010) 035003

OUTLINE

- We investigate the proposition that the "instability" structures observed in the experiments constitute in reality new equilibrium states with 3D character; an axisymmetric boundary is imposed
- 3D magnetohydrodynamic (MHD) fixed boundary equilibria with imposed nested flux surfaces are investigated with:
  VMEC2000
  –S. P. Hirshman, O. Betancourt, J. Comput. Phys. **96** (1991) 99
  ANIMEC
  –W. A. Cooper et al., Comput. Phys. Commun. **180** (2009) 1524
- MHD equilibria with 3D internal helical structures computed for TCV, ITER (hybrid scenario), MAST, JET (Snakes) and RFX-mod
- Linear ideal MHD stability computed with TERPSICHORE for RFX-mod
  –D. V. Anderson et al., Int. J. Supercomp. Appl. **4** (1990) 33

Magnetohydrodynamic Equilibria — 3D

- Impose nested magnetic surfaces and single magnetic axis
- Minimise energy of the system

$$W = \int\int\int d^3x \left(\frac{B^2}{2\mu_0} + \frac{p_{\|}(s,B)}{\Gamma - 1} \right)$$

- Solve inverse equilibrium problem : $R = R(s,u,v)$, $Z = Z(s,u,v)$.

- Variation of the energy

$$\begin{aligned} \frac{dW}{dt} = & - \int\int\int ds du dv \left[F_R \frac{\partial R}{\partial t} + F_Z \frac{\partial Z}{\partial t} + F_\lambda \frac{\partial \lambda}{\partial t} \right] \\ & - \int\int_{s=1} du dv \left[R \left(p_\perp + \frac{B^2}{2\mu_0} \right) \left(\frac{\partial R}{\partial u}\frac{\partial Z}{\partial t} - \frac{\partial Z}{\partial u}\frac{\partial R}{\partial t} \right) \right] \end{aligned}$$

Magnetohydrodynamic Equilibria — 3D

- The MHD forces are

$$
\begin{aligned}
F_R = \quad & \frac{\partial}{\partial u}[\sigma\sqrt{g}B^u(\boldsymbol{B}\cdot\boldsymbol{\nabla}R)] + \frac{\partial}{\partial v}[\sigma\sqrt{g}B^v(\boldsymbol{B}\cdot\boldsymbol{\nabla}R)] \\
- \quad & \frac{\partial}{\partial u}\Big[R\frac{\partial Z}{\partial s}\Big(p_\perp + \frac{B^2}{2\mu_0}\Big)\Big] + \frac{\partial}{\partial s}\Big[R\frac{\partial Z}{\partial u}\Big(p_\perp + \frac{B^2}{2\mu_0}\Big)\Big] \\
+ \quad & \frac{\sqrt{g}}{R}\Big[\Big(p_\perp + \frac{B^2}{2\mu_0}\Big) - \sigma R^2 (B^v)^2\Big] \\
F_z = \quad & \frac{\partial}{\partial u}[\sigma\sqrt{g}B^u(\boldsymbol{B}\cdot\boldsymbol{\nabla}Z)] + \frac{\partial}{\partial v}[\sigma\sqrt{g}B^v(\boldsymbol{B}\cdot\boldsymbol{\nabla}Z)] \\
+ \quad & \frac{\partial}{\partial u}\Big[R\frac{\partial R}{\partial s}\Big(p_\perp + \frac{B^2}{2\mu_0}\Big)\Big] - \frac{\partial}{\partial s}\Big[R\frac{\partial R}{\partial u}\Big(p_\perp + \frac{B^2}{2\mu_0}\Big)\Big]
\end{aligned}
$$

- The λ force equation minimises the spectral width and corresponds to the binormal projection of the momentum balance at the equilibrium state.

$$
F_\lambda = \Phi'(s)\Big[\frac{\partial(\sigma B_v)}{\partial u} - \frac{\partial(\sigma B_u)}{\partial v}\Big]
$$

- For isotropic pressure $p_\parallel = p_\perp = p$ and $\sigma = 1/\mu_0$.

Magnetohydrodynamic Equilibria — 3D

- Use Fourier decomposition in the periodic angular variables u and v and a special finite difference scheme for the radial discretisation
- An accelerated steepest descent method is applied with matrix preconditioning to obtain the equilibrium state
- The radial force balance is a diagnostic of the accuracy of the equilibrium state in this approach

$$\left\langle \frac{F_s}{\Phi'(s)} \right\rangle = -\left\langle \frac{1}{\Phi'(s)} \frac{\partial p_{\|}}{\partial s}\Big|_B \right\rangle - \frac{\partial}{\partial s}\left\langle \frac{\sigma B_v}{\sqrt{g}} \right\rangle - \iota(s)\frac{\partial}{\partial s}\left\langle \frac{\sigma B_u}{\sqrt{g}} \right\rangle$$

- $\langle \cdots \rangle$ denotes a flux surface average

$$\langle A \rangle = \frac{L}{(2\pi)^2} \int_0^{2\pi/L} dv \int_0^{2\pi} du \sqrt{g} A(s,u,v)$$

- This model is implemented in the ANIMEC code, an anisotropic pressure extension of the VMEC2000 code. L is the number of toroidal field periods.

Boundaries for TCV, ITER, MAST and JET

- Fixed axisymmetric boundary equilibrium studies are explored.
- TCV boundary description: $R_b = 0.8 + 0.2\cos u + 0.06\cos 2u; \quad Z_b = 0.48\sin u$
- MAST, JET boundary: $R_b = R_0 + a\cos(u + \delta\sin u + \tau\sin 2u); \quad Z_b = Ea\sin u$
  MAST: $R_0 = 0.9m,\ a = 0.54m,\ E = 1.744,\ \delta = 0.3985,\ \tau = 0.1908$
  JET: $R_0 = 2.96m,\ a = 1.25m,\ E = 1.68,\ \delta = 0.3,\ \tau = 0$

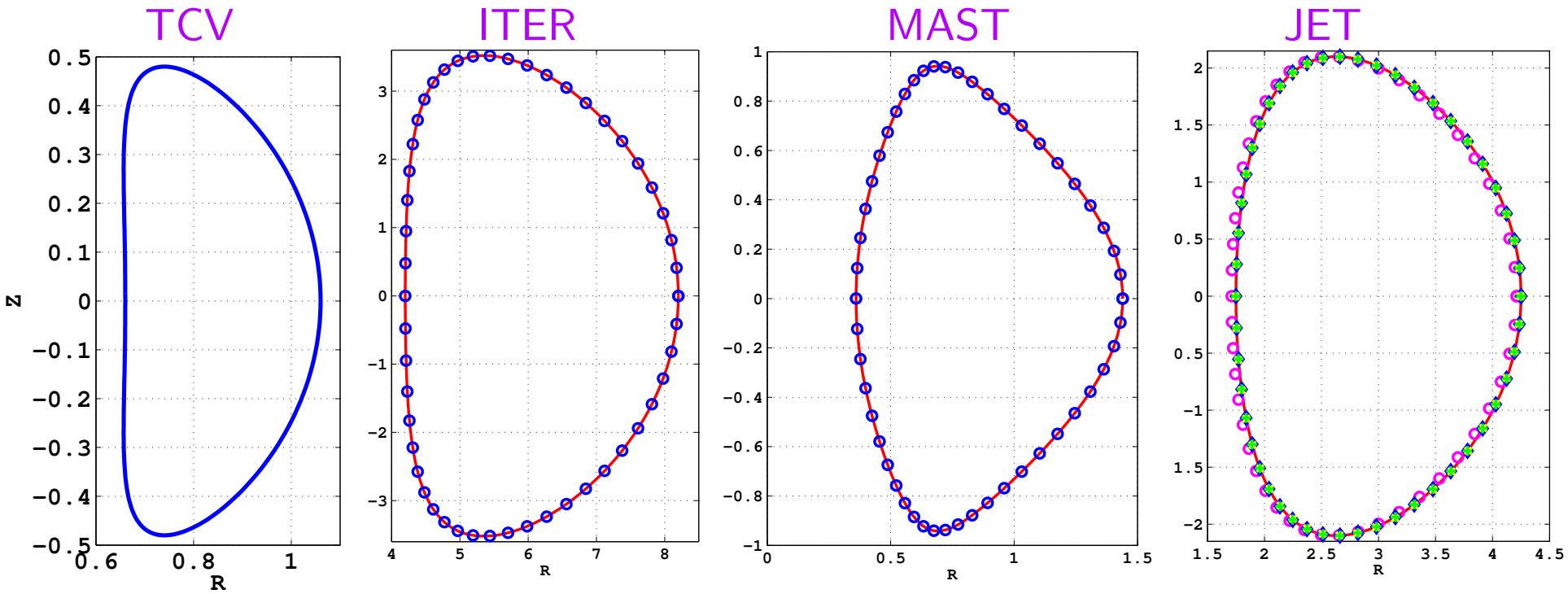

Bifurcated equilibria in TCV

- Selection of q-profiles that yield bifurcated equilibria in TCV.
- Boundary description: $R_b = 0.8 + 0.2\cos u + 0.06\cos 2u, \quad Z_b = 0.48\sin u.$
- $q = (0.5+s-1.1s^4)^{-1}$, $(0.7+0.7s-s^4)^{-1}$, $(0.9+0.2s-0.8s^6)^{-1}$, $(0.98-0.7s^9)^{-1}$.

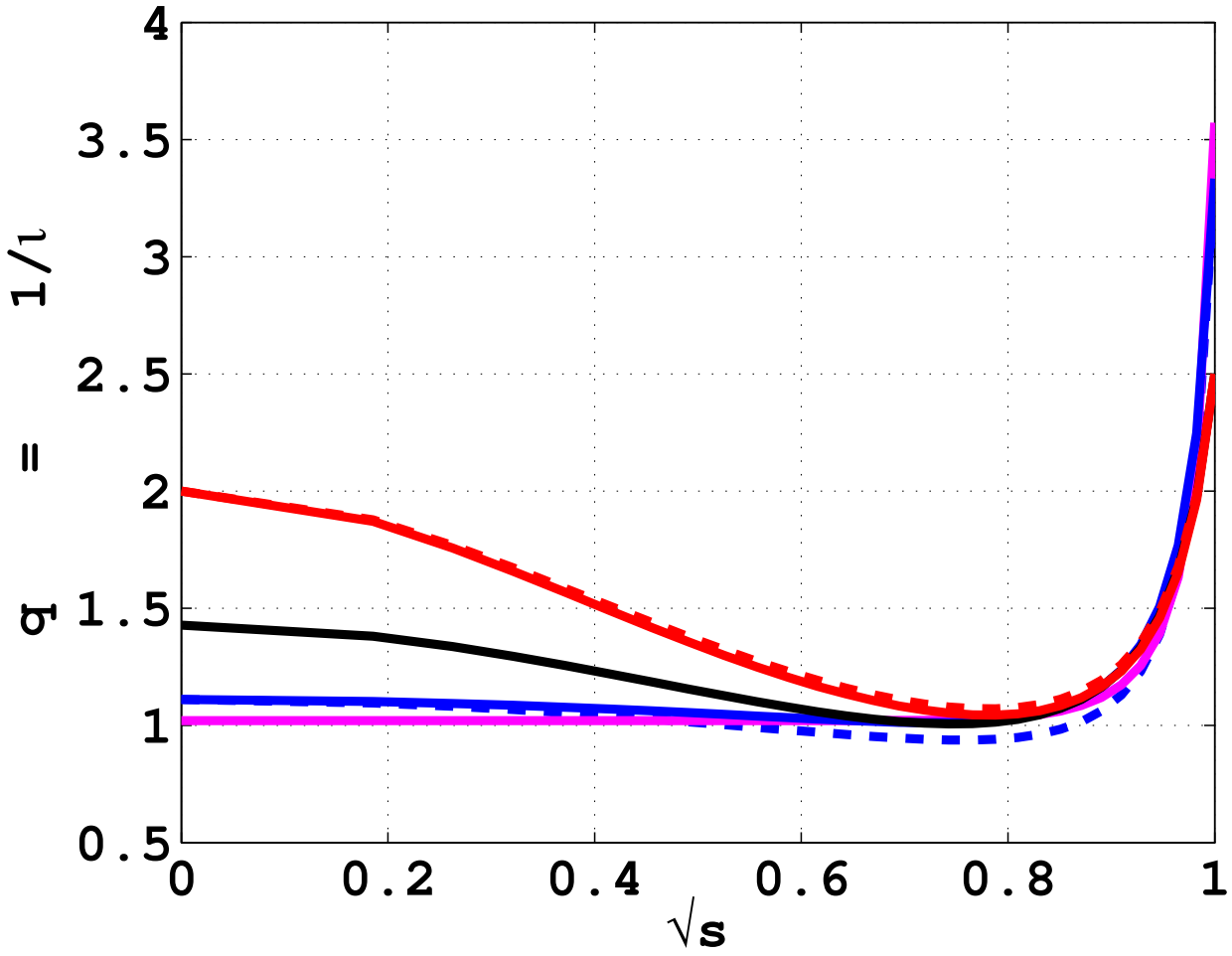

TCV toroidal flux contours at various cross sections

- TCV toroidal magnetic flux contours with prescribed $\iota = 0.9 + 0.2s - 0.8s^6$ profile.

Axisymmetric

$v = 0$ $v = \pi/3$ $v = 2\pi/3$ $v = \pi$

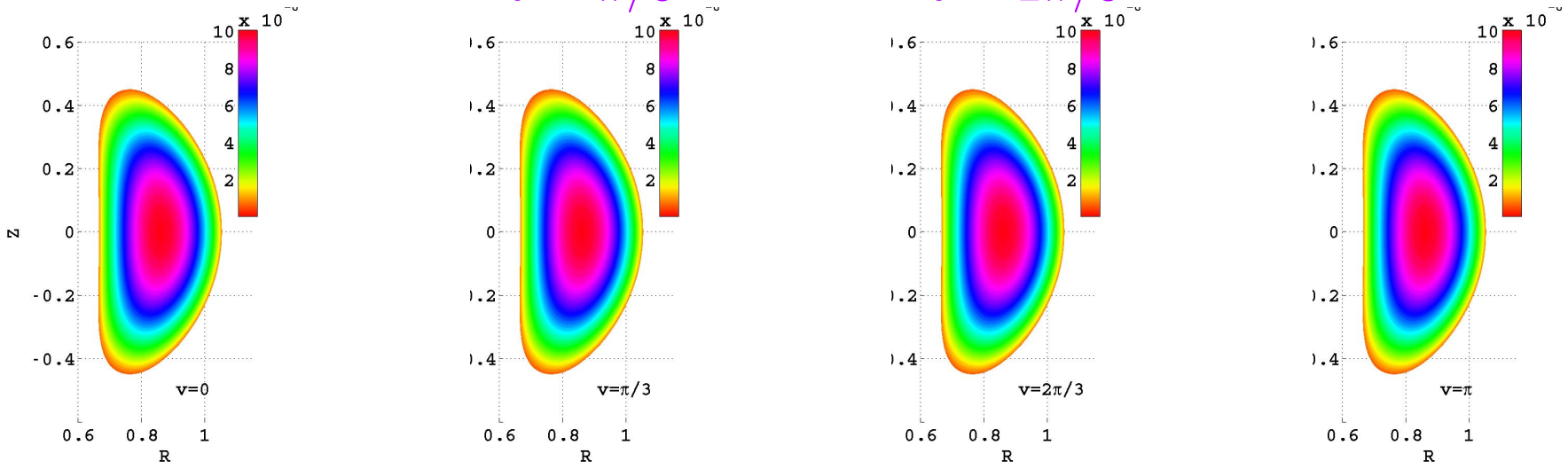

Helical

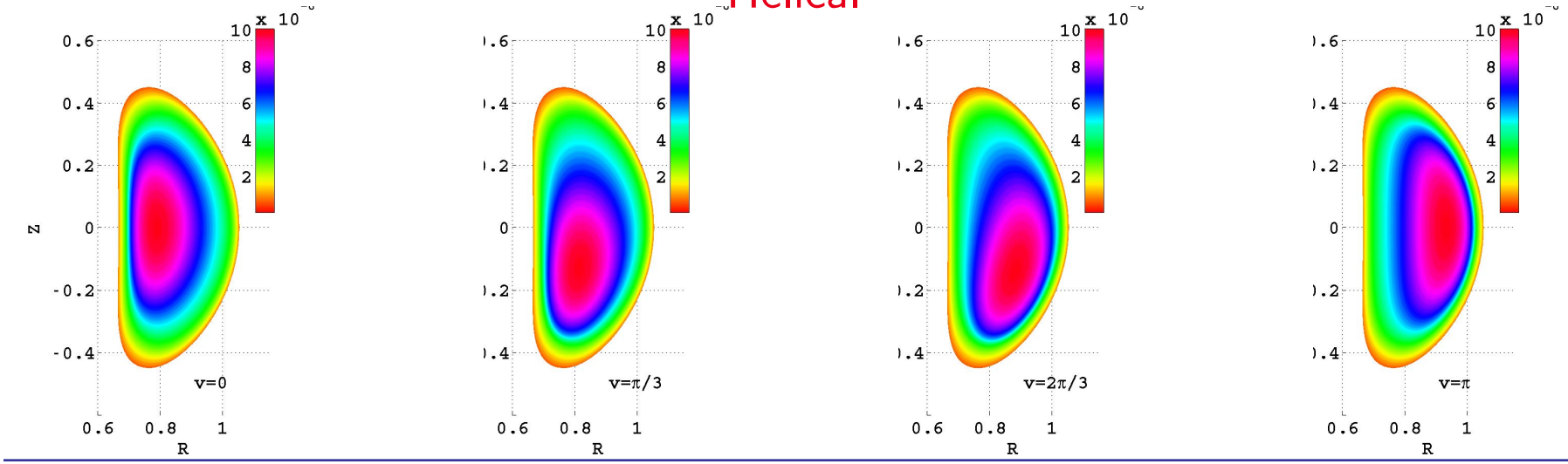

Helical equilibrium structures in TCV

- Helical axis displacement and energy difference as function of q_{min}.
- $q(s) = [0.9 + \alpha_1 s - (0.6 + \alpha_1)s^6]^{-1}, \qquad \alpha_1 = 0.16 \rightarrow 0.32.$
- $R_{01}(0); Z_{01}(0)$ $\qquad\qquad$ $\mu_0(W_{hel} - W_{axi})$

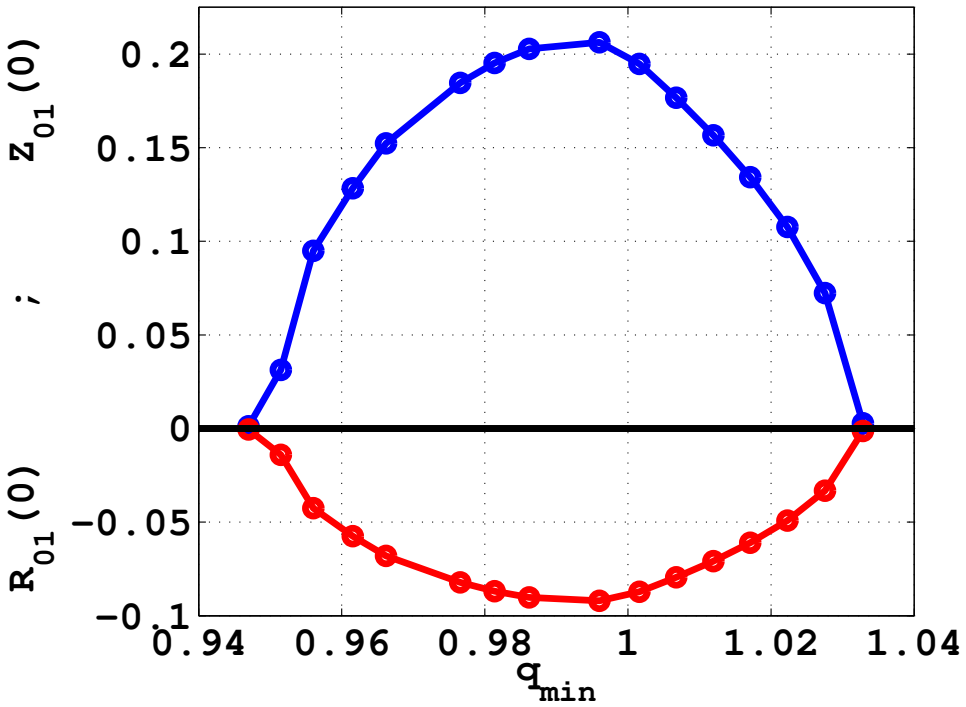

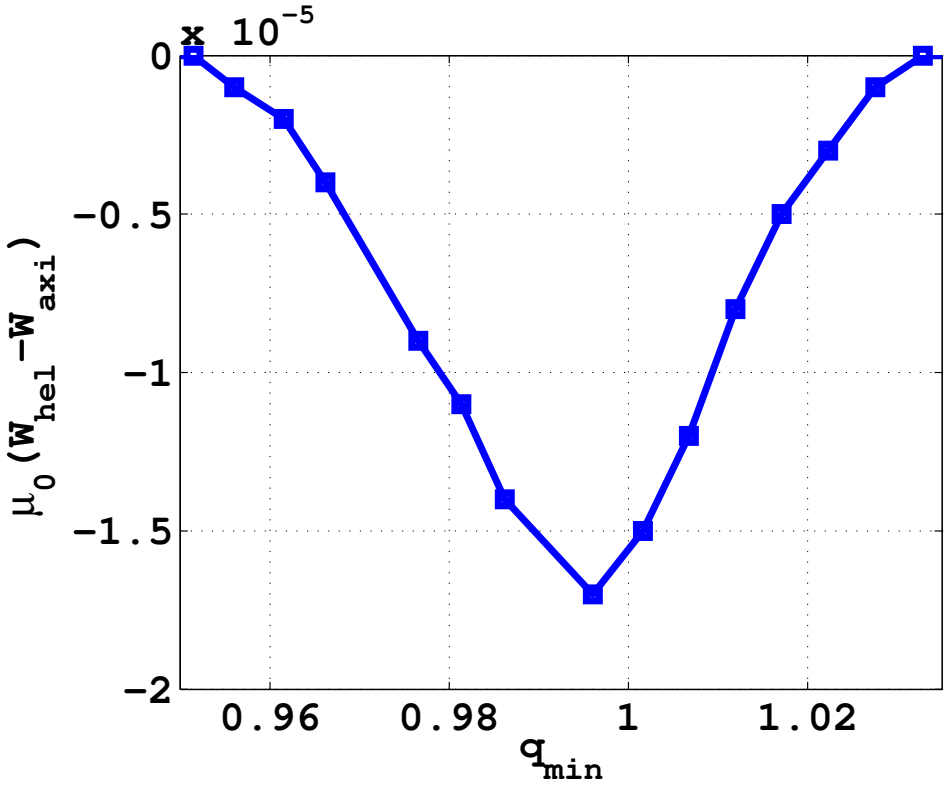

TCV helical structures at finite $\langle\beta\rangle$

- Flat core pressure and q-profile with weak shear reversal
- $q(s) = (0.9 + 0.3s - s^4)^{-1}$.
  $p(s) = p_0(1 + 0.410227s^2 - 14.1988s^4 + 29.6253s^6 - 22.9512s^8 + 6.1152s^{10})$.
- p, q-profiles

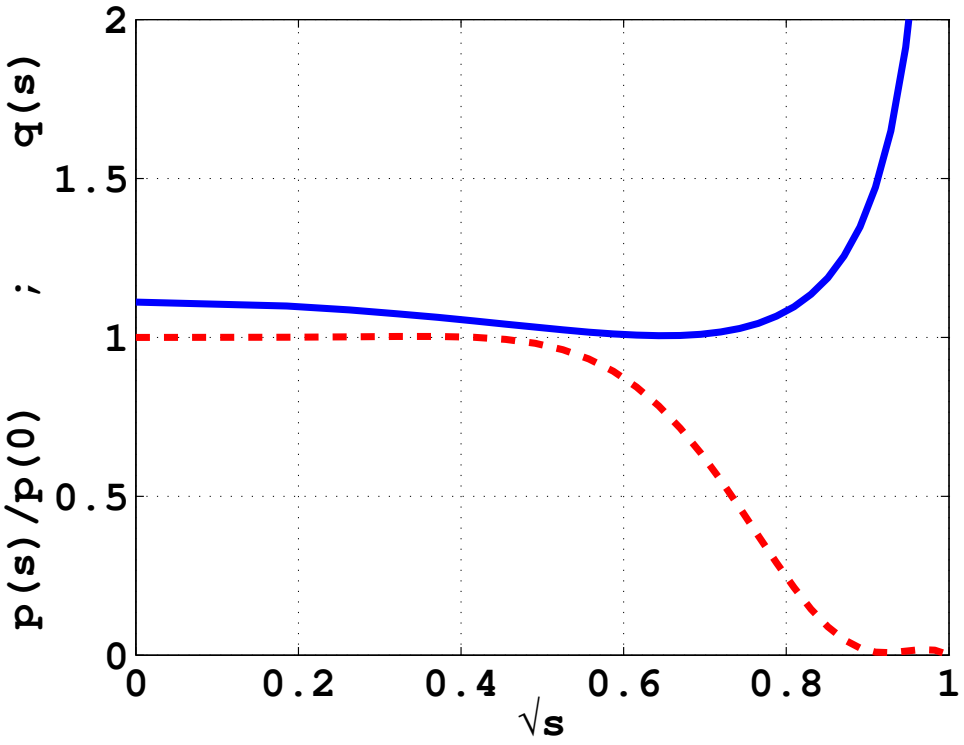

$R_{01}(0); Z_{01}(0)$

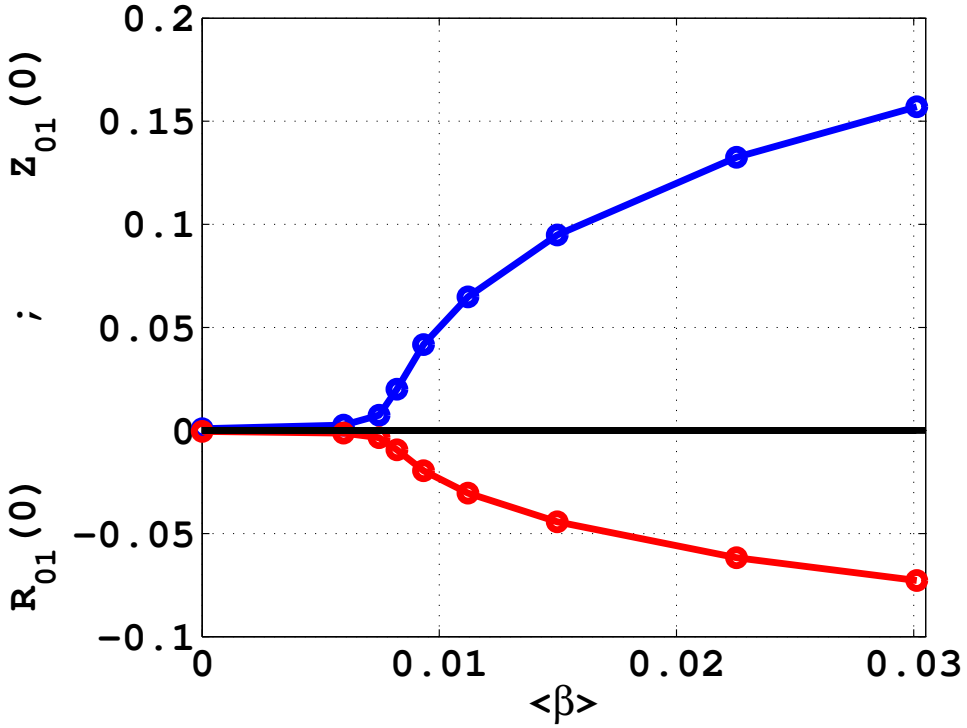

ITER equilibrium profiles

- Prescribe mass profile and toroidal current profile. $p(s) \sim \mathcal{M}(s)[\Phi'(s)]^{\Gamma}$
- Equilibria have toroidal current $13 - 14MA$, $B_t = 4.6T$, $\langle\beta\rangle \simeq 2.9\%$
- q-profile

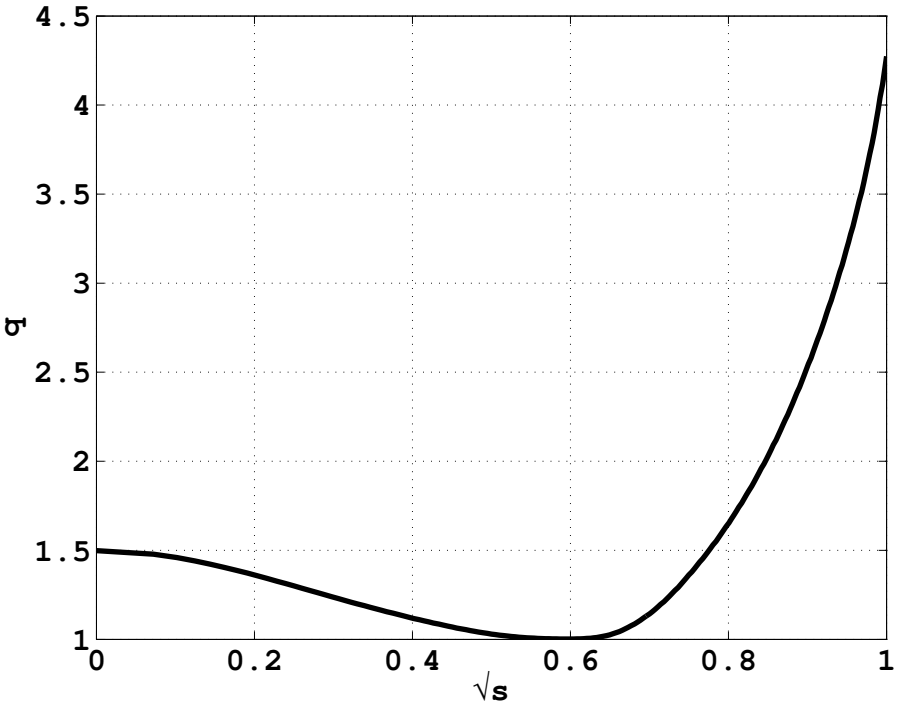

q-profile range for helical states

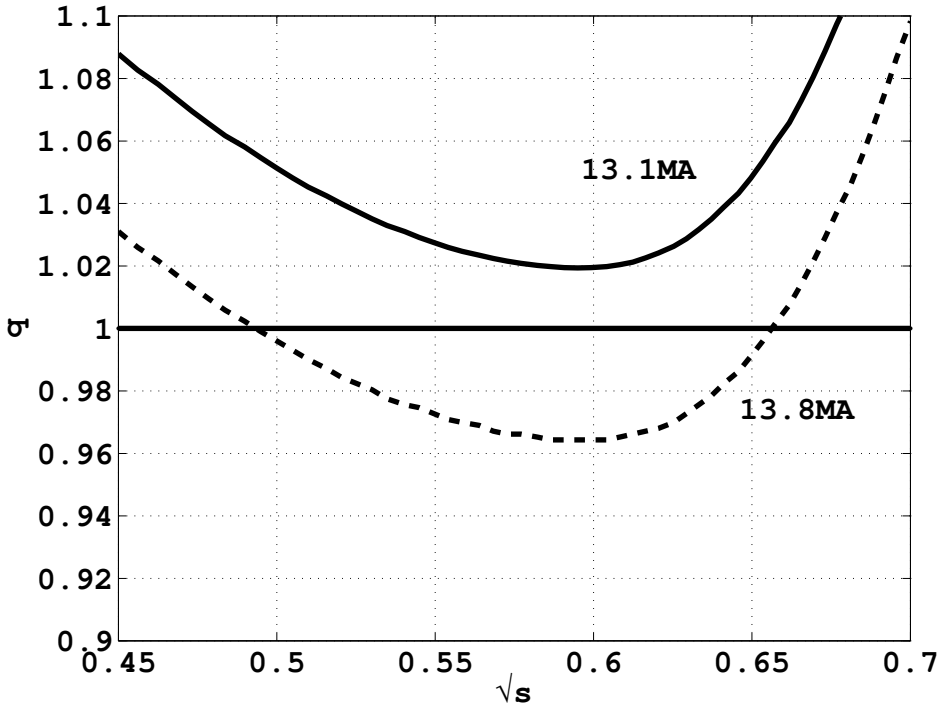

ITER pressure contours at various cross sections

- Contours of constant pressure of an ITER hybrid scenario equilibrium with $13.3MA$ toroidal plasma current

$v = 0$ $v = \pi/3$ $v = 2\pi/3$ $v = \pi$

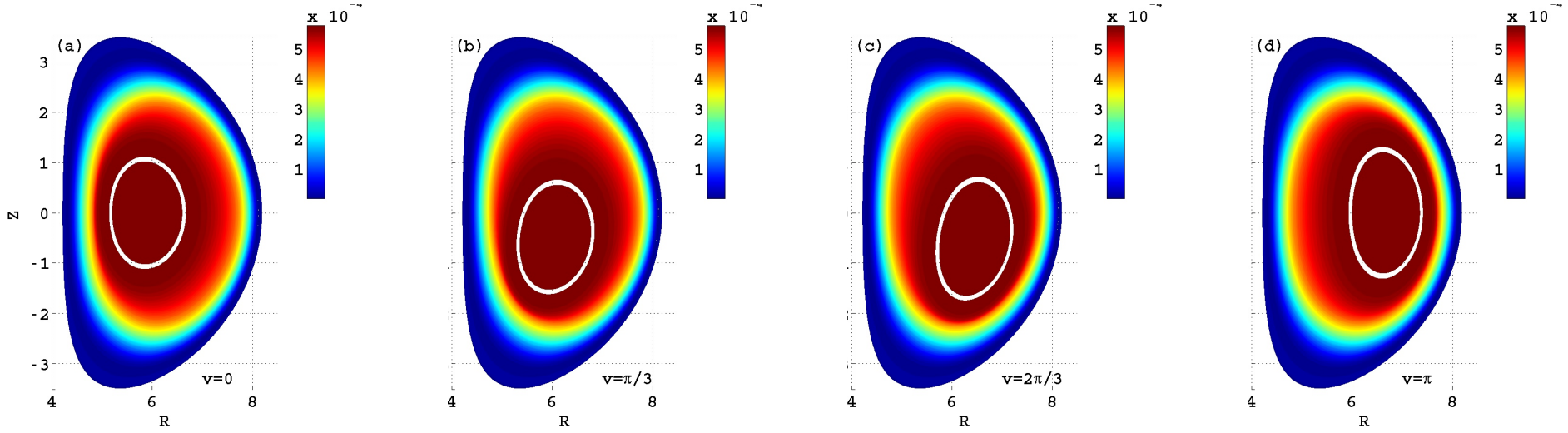

Convergence of solutions

- Define helical excursion parameter

$$\delta_H = \frac{\sqrt{R_{01}^2(s=0) + Z_{01}^2(s=0)}}{a}$$

- Convergence of δ_H with N_r = number of radial grid points

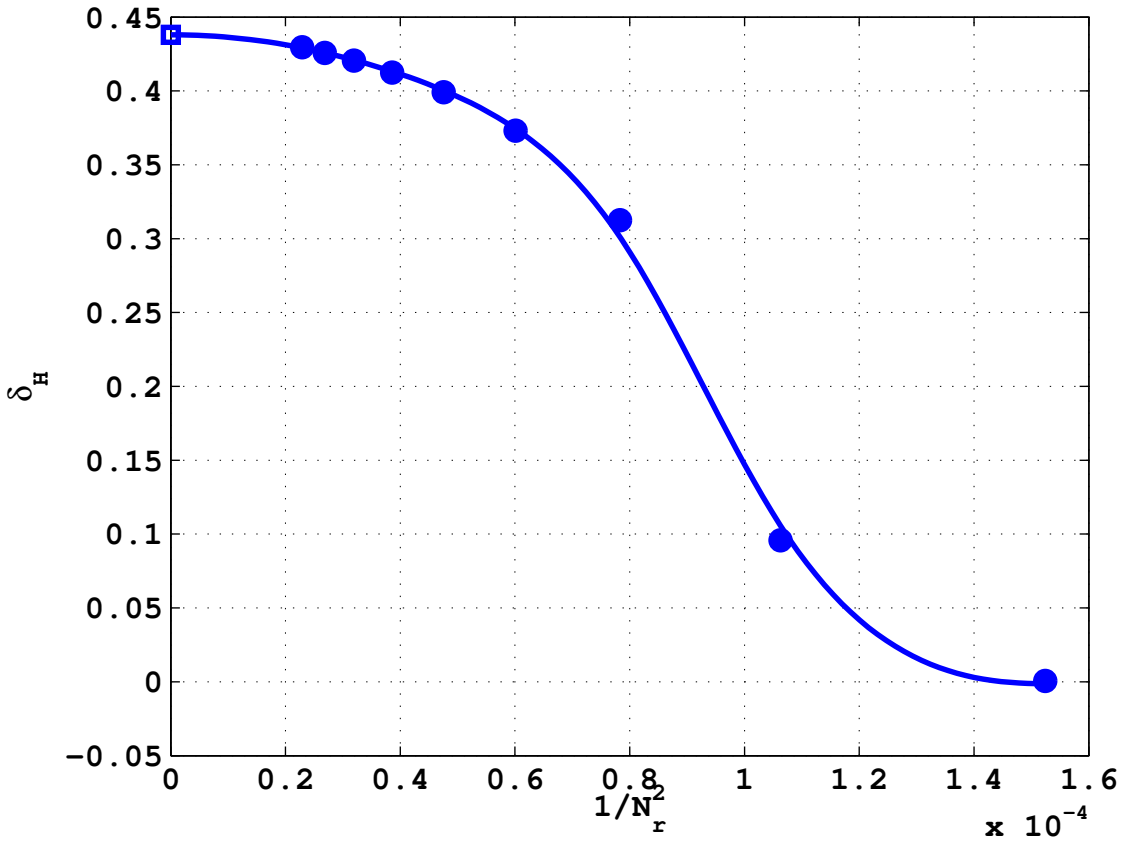

Helical core ITER equilibria

- Variation of the helical axis distortion parameter δ_H with respect to the toroidal current and corresponding variation with respect to q_{min}.

- δ_H versus current

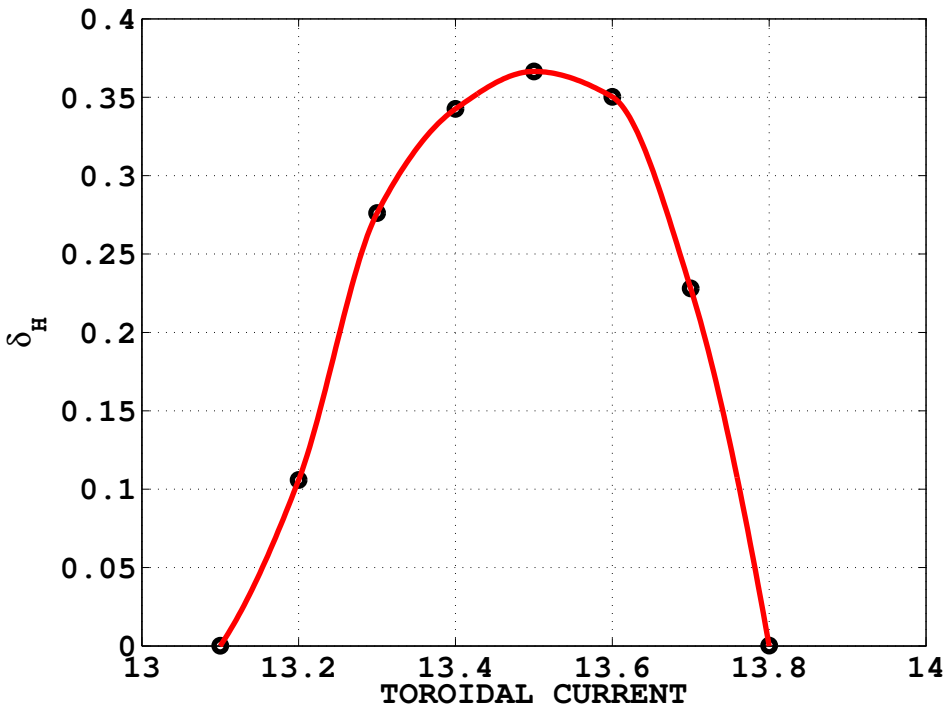

- δ_H versus q_{min}

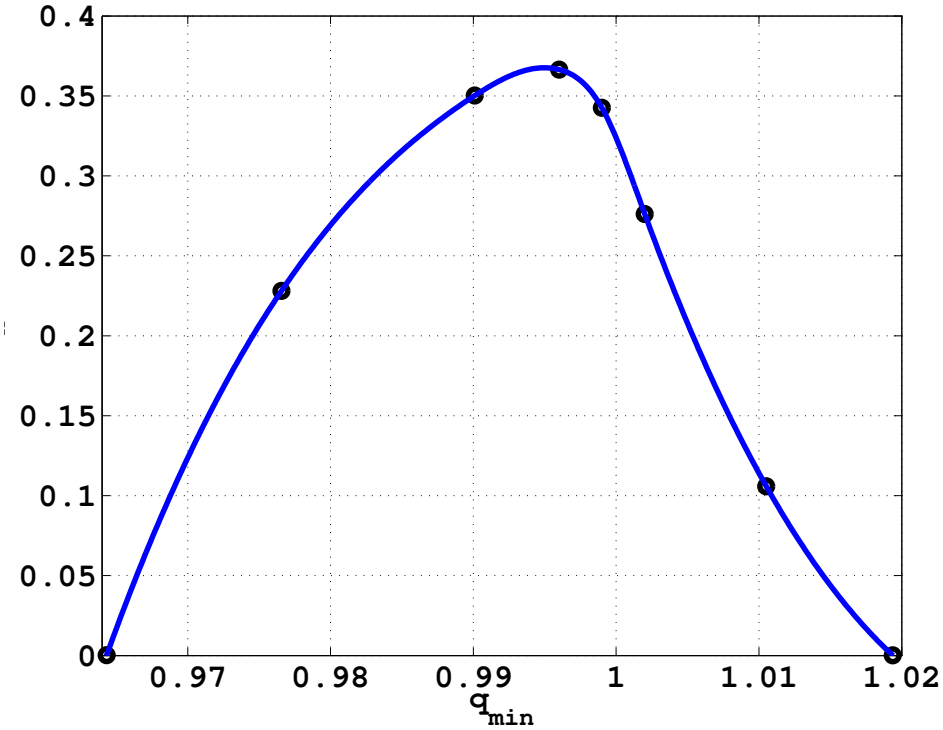

ITER pressure contours as a function of plasma current

- Contours of constant pressure at the cross section with toroidal angle $v = 2\pi/3$

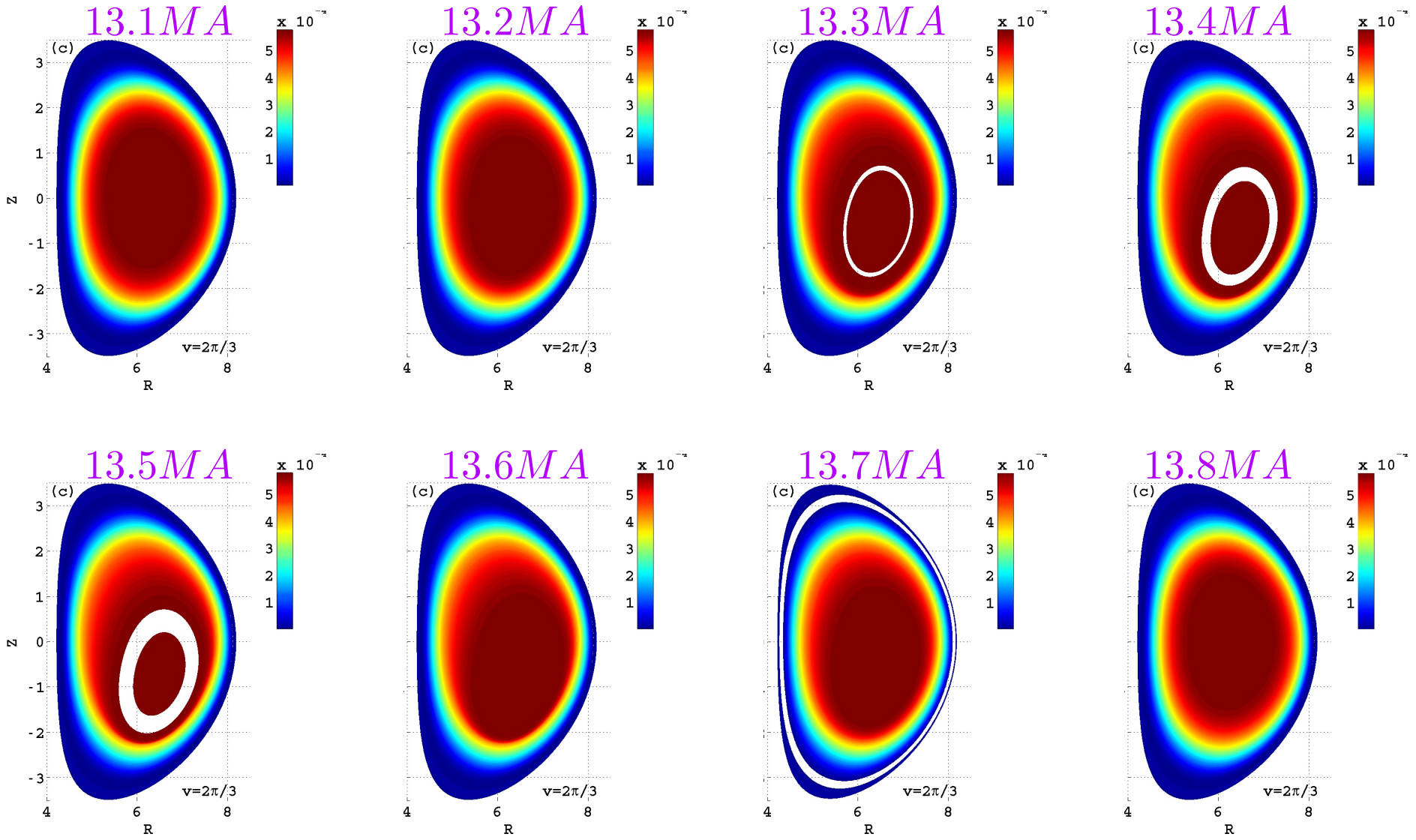

Finite $\langle\beta\rangle$ ITER scan

- The ITER hybrid scenario is projected in the range $12 - 14MA$ with $B_t = 5.3T$. With a sharper core concentrated toroidal current at $12MA$, the variation of the helical axis distortion parameter δ_H with respect to $\langle\beta\rangle$ is computed.

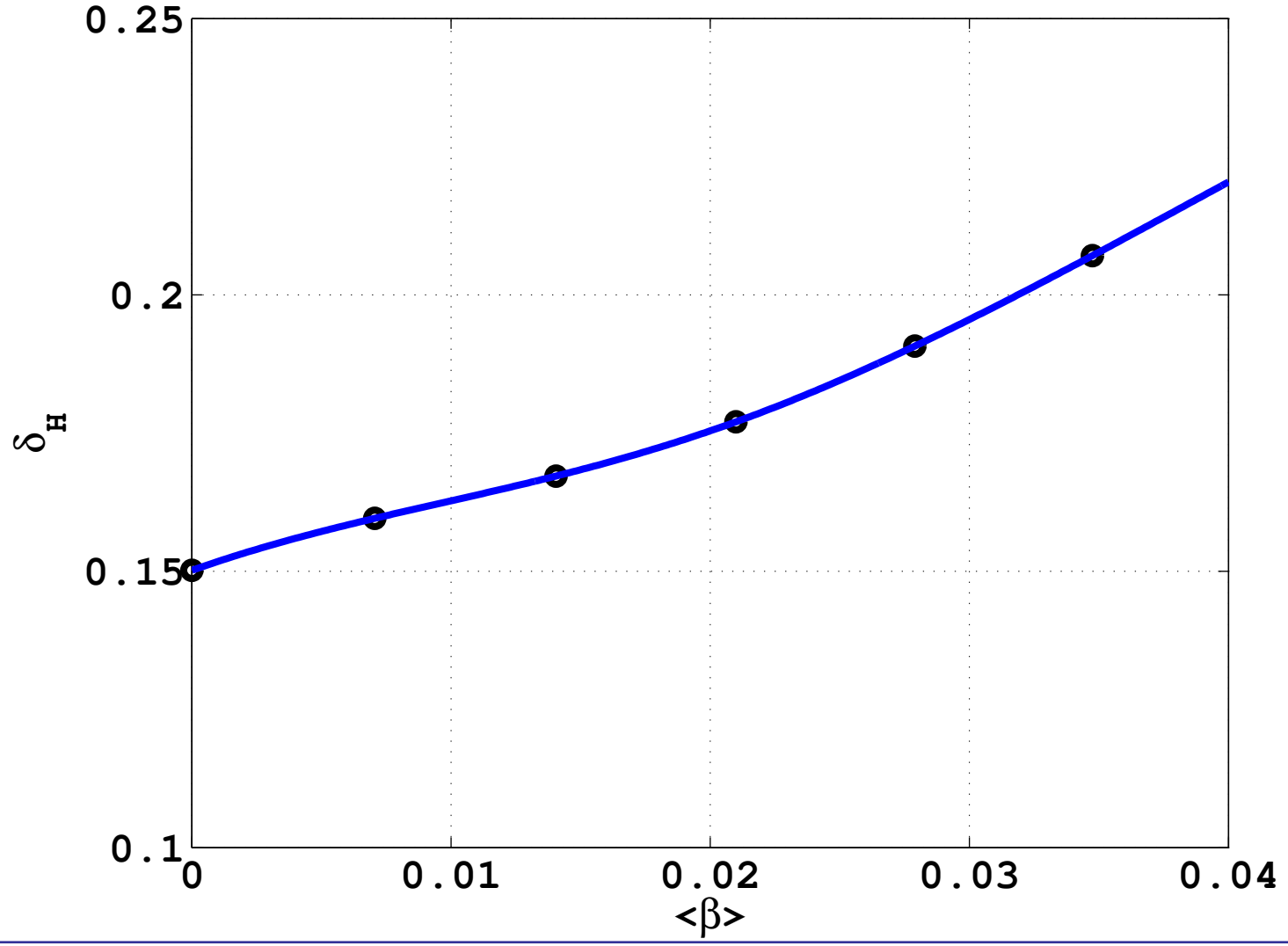

MAST pressure contours at various cross sections

- Contours of constant pressure of a MAST equilibrium

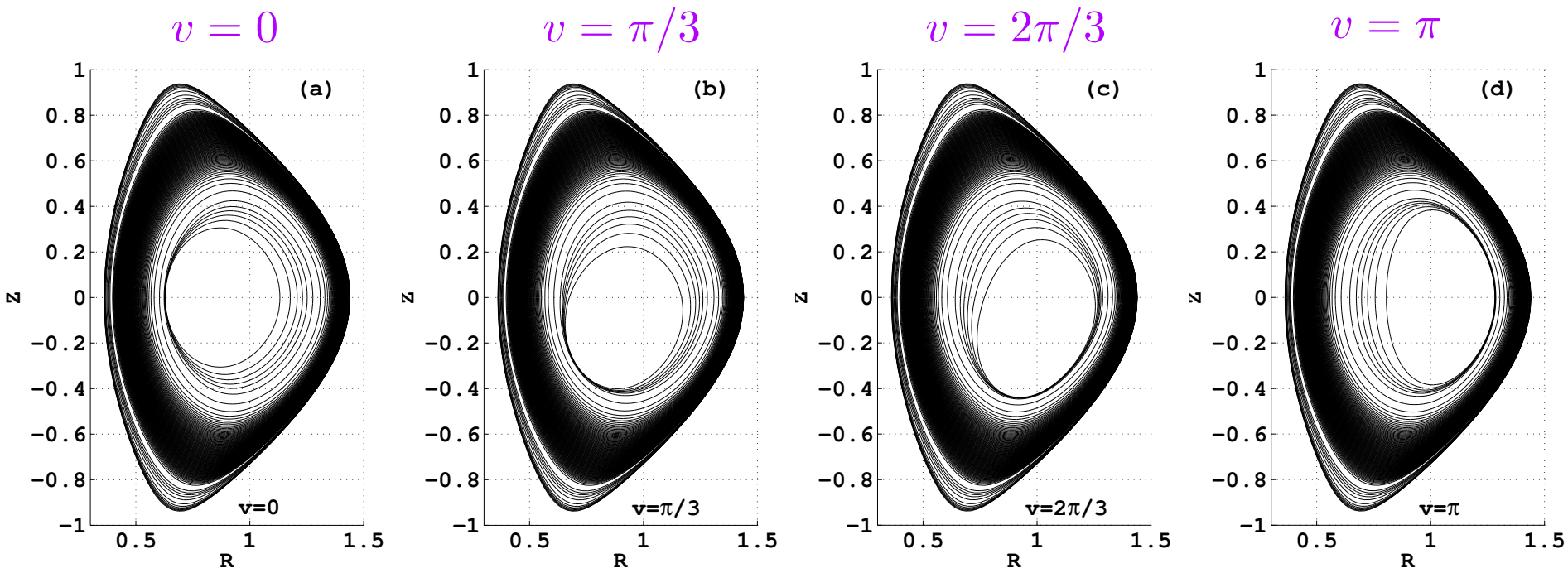

- This serves as a model for long-lived modes in MAST
  -I.T. Chapman et al., Nucl. Fusion **50** (2010) 045997

- Saturated internal kinks also observed on NSTX
  -J.E. Menard et al., Nucl. Fusion **45** (2005) 539

JET "snake" equilibrium profiles

- Prescribe mass profile and toroidal current profile.
- Equilibrium has toroidal current $3.85MA$, $B_t = 3.1T$, $\langle\beta\rangle \simeq 2.3\%$
- pressure profile

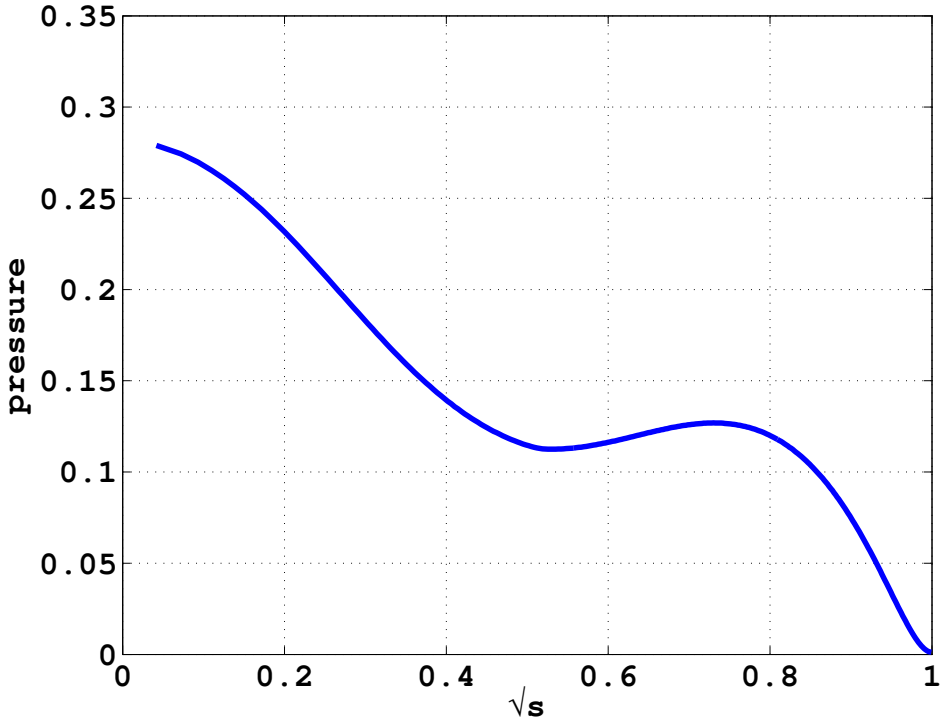

q-profile

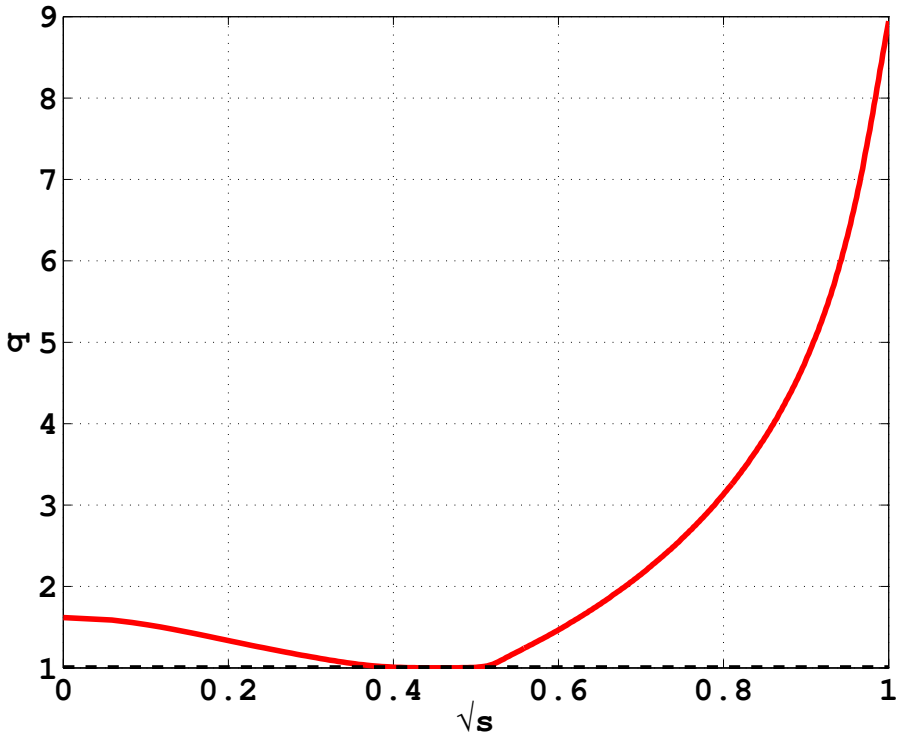

JET pressure, mod-B contours at various cross sections

- Contours of constant pressure and mod-B of a JET "snake" equilibrium

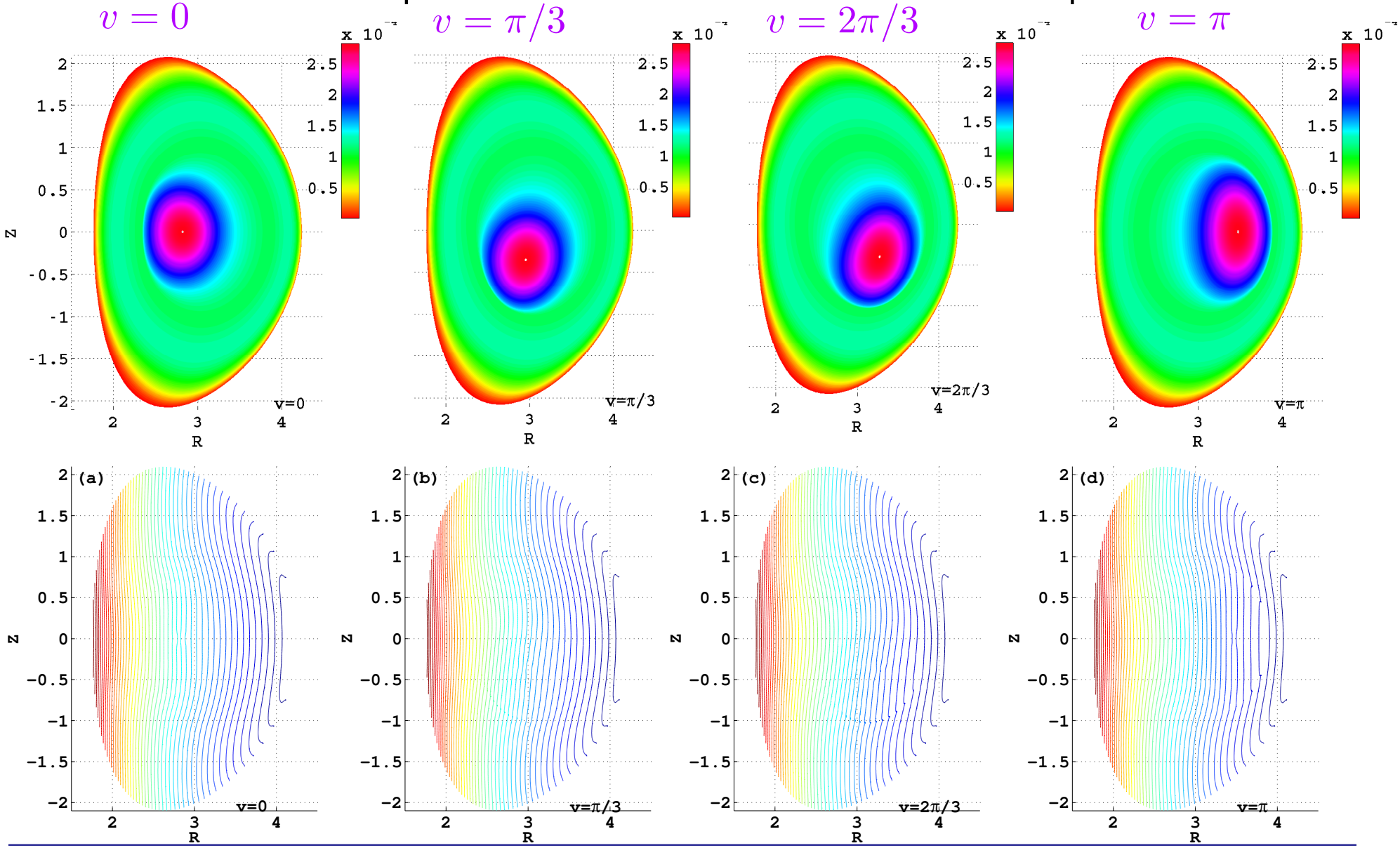

JET "snake" equilibrium structure

- Standard view of a snake (with variation with respect to toroidal angle in lieu of time in the simulation).

- experiment (courtesy of A. Weller)

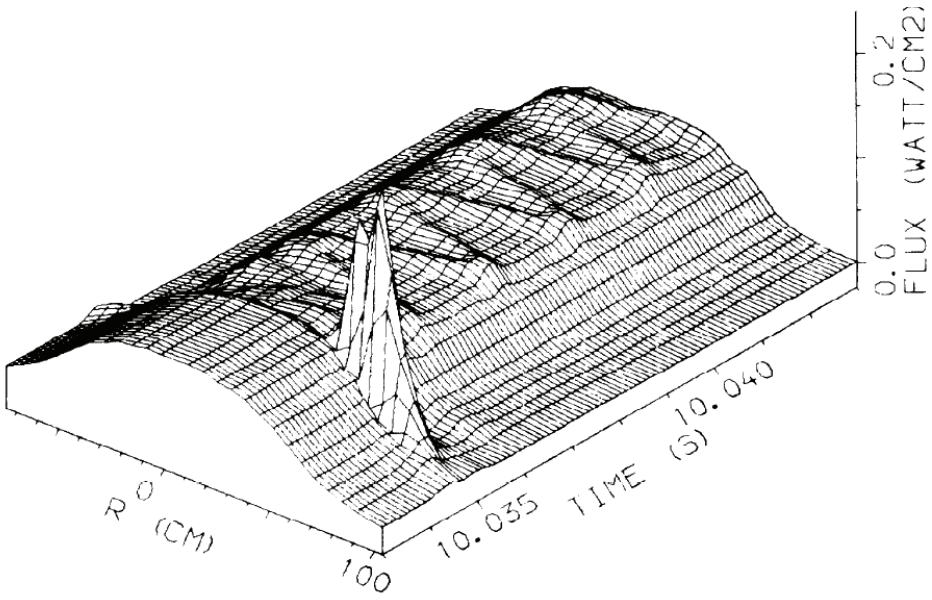

ANIMEC simulation

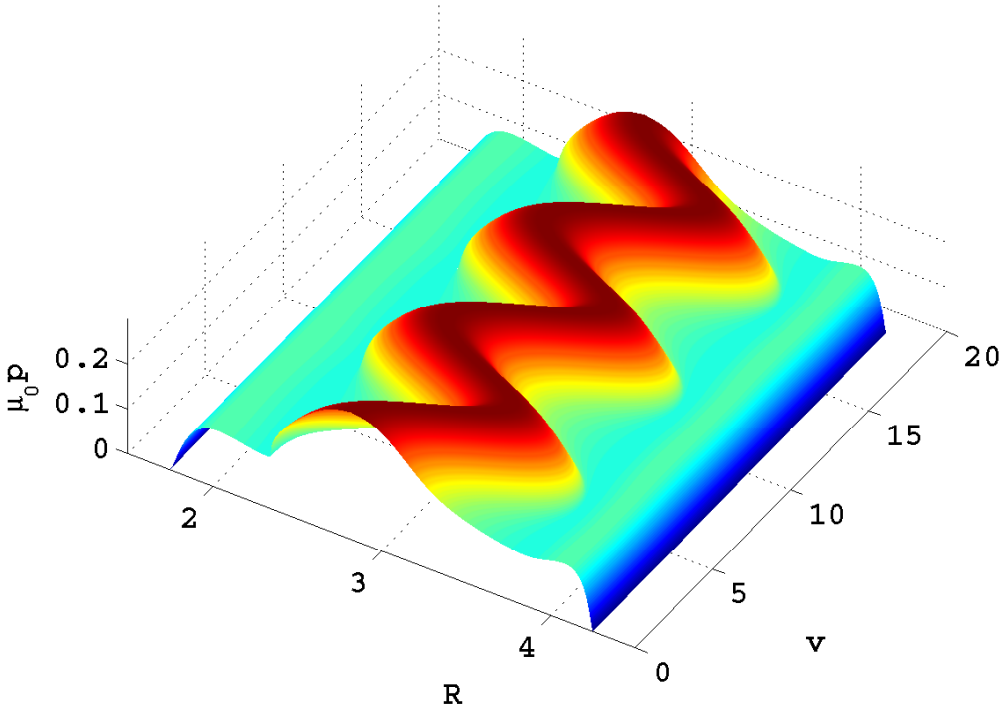

RFX-mod toroidal flux and $j \cdot B/B^2$ contours

- Contours of constant toroidal flux (VMEC coordinates) and $\boldsymbol{j} \cdot \boldsymbol{B}/B^2$ (Boozer coordinates) in a RFX-mod SHAx equilibrium state

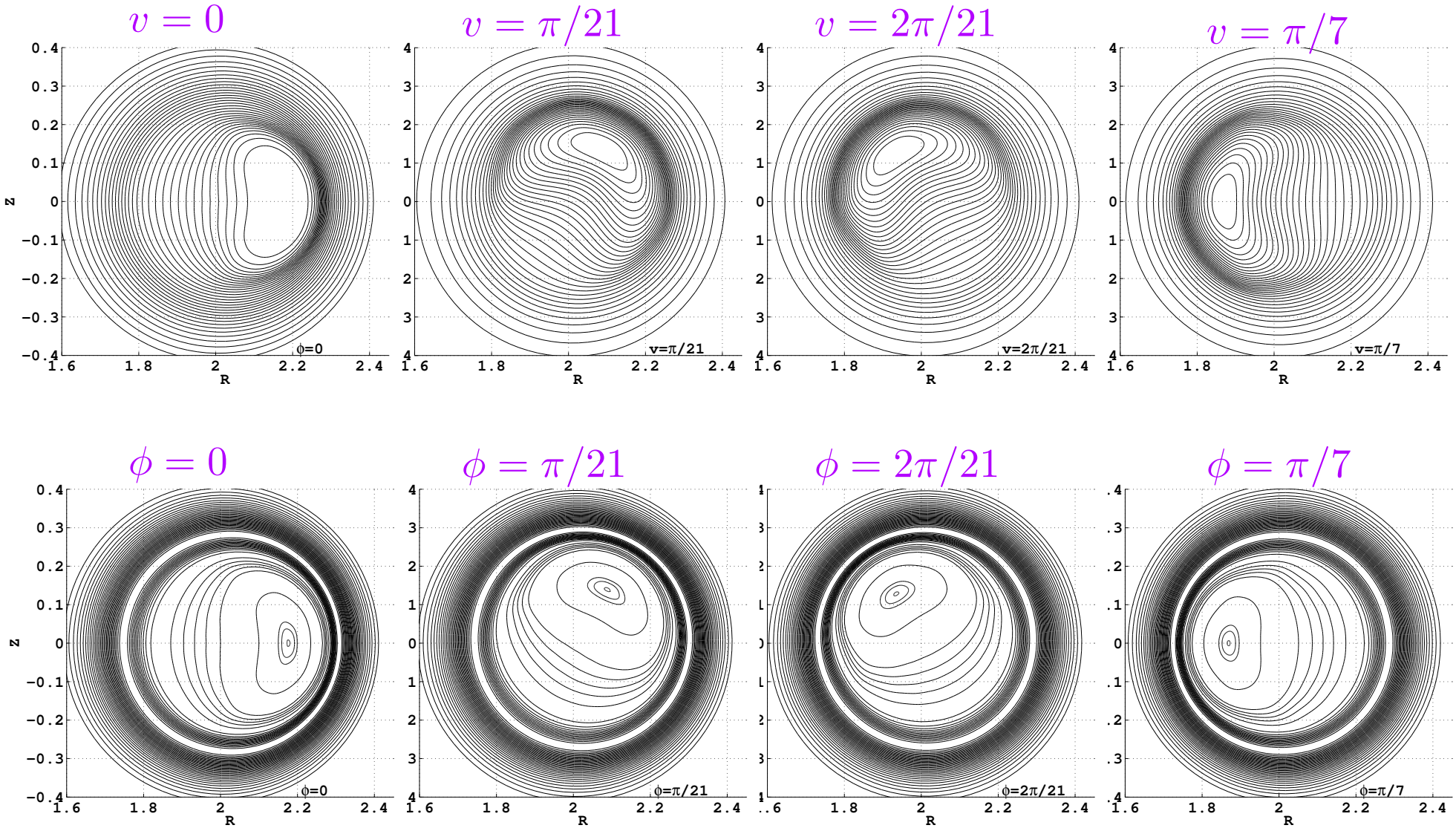

RFX-mod toroidal flux and mod-B contours

- Contours of constant toroidal flux and mod-B in the Boozer coordinate frame for the RFX-mod SHAx equilibrium state

$\phi = 0$ $\phi = \pi/21$ $\phi = 2\pi/21$ $\phi = \pi/7$

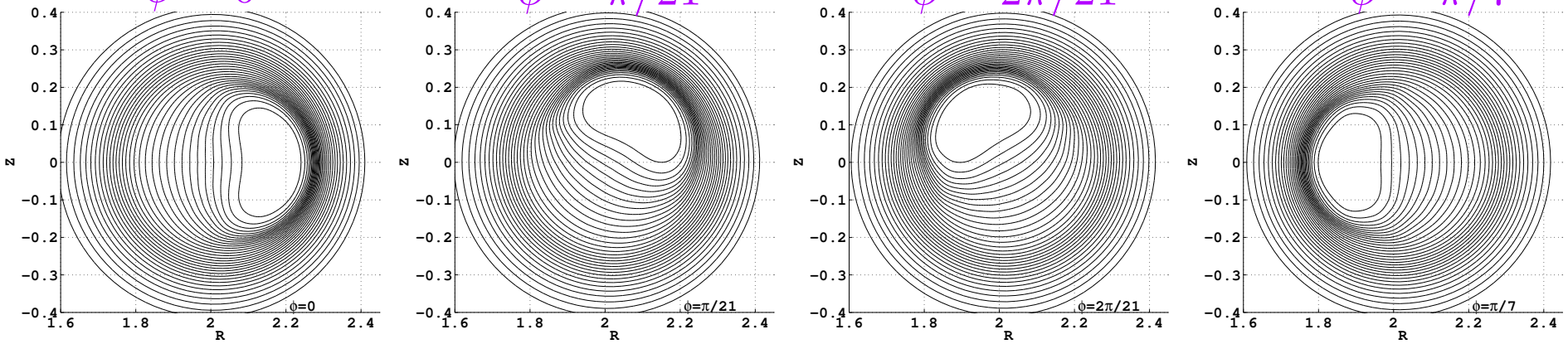

$\phi = 0$ $\phi = \pi/21$ $\phi = 2\pi/21$ $\phi = \pi/7$

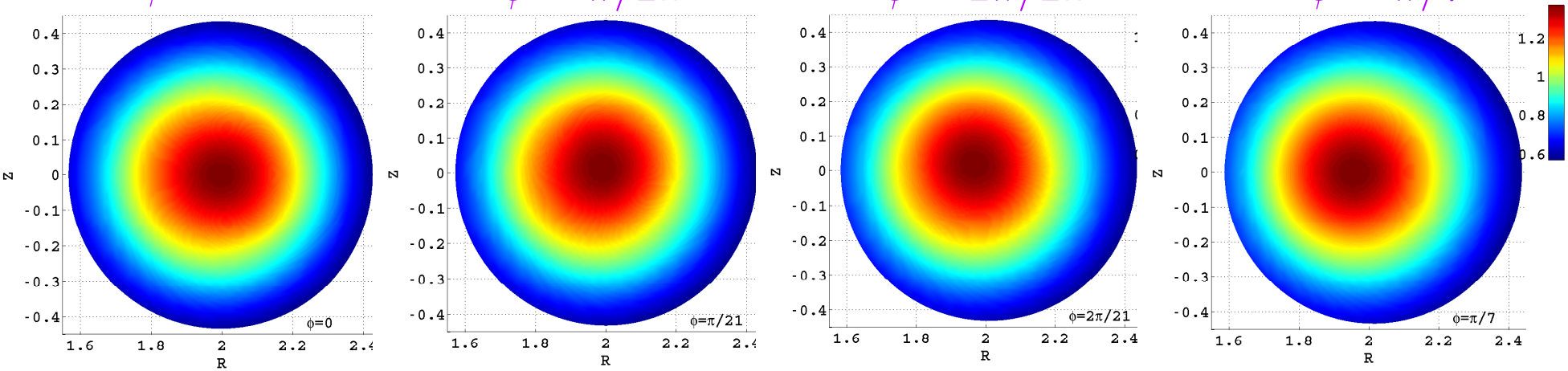

Mod-B^2 Fourier amplitudes in RFX-mod

- Dominant Fourier amplitudes of B^2 in the RFX-mod SHAx equilibrium state

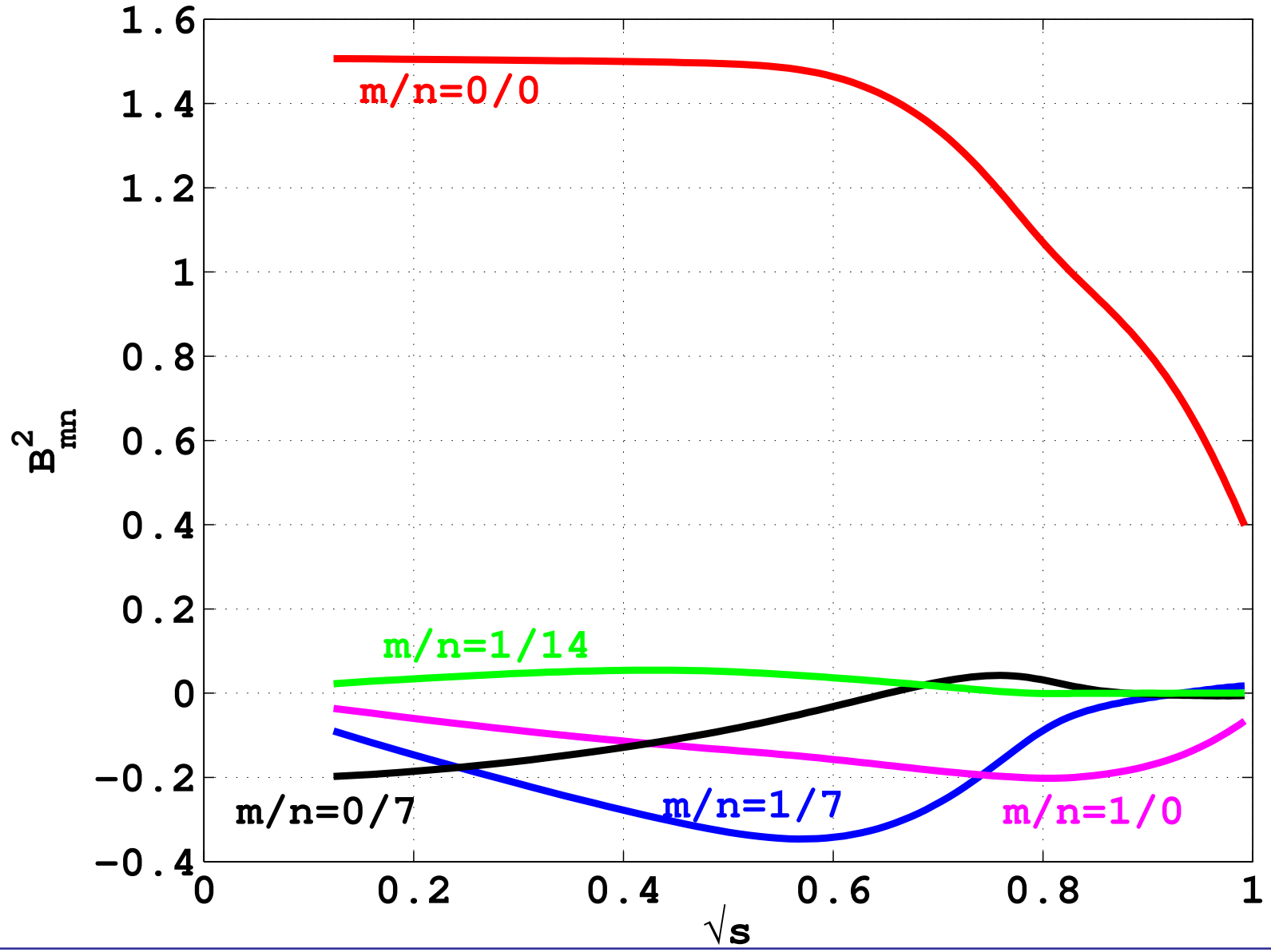

Linear Ideal MHD Stability

- Internal potential energy

$$\delta W_p = \frac{1}{2}\int\int\int d^3x \left[C^2 + \Gamma p |\boldsymbol{\nabla}\cdot\boldsymbol{\xi}|^2 - D|\boldsymbol{\xi}\cdot\boldsymbol{\nabla}s|^2\right]$$

- Use Boozer coordinates

$$\boldsymbol{\xi} = \sqrt{g}\xi^s \boldsymbol{\nabla}\theta \times \boldsymbol{\nabla}\phi + \eta\frac{(\boldsymbol{B}\times\boldsymbol{\nabla}s)}{B^2} + \left[\frac{J(s)}{\Phi'(s)B^2}\eta - \mu\right]\boldsymbol{B}$$

- Fourier decomposition in angular variables

$$\begin{aligned}\xi^s(s,\theta,\phi) &= \sum_\ell s^{-q_\ell} X_\ell(s) sin(m_\ell\theta - n_\ell\phi + \Delta)\\ \eta(s,\theta,\phi) &= \sum_\ell Y_\ell(s) cos(m_\ell\theta - n_\ell\phi + \Delta)\end{aligned}$$

- A hybrid finite element method is applied for the radial discretisation. In the 3D TERPSICHORE stability code, COOL finite elements based on variable order Legendre polynomials have been implemented. The order of the polynomial is labelled with p.

MHD stability in RFX-mod

- Ideal MHD stability with respect to $n = 8$ family of modes $(w/a = 1.099)$

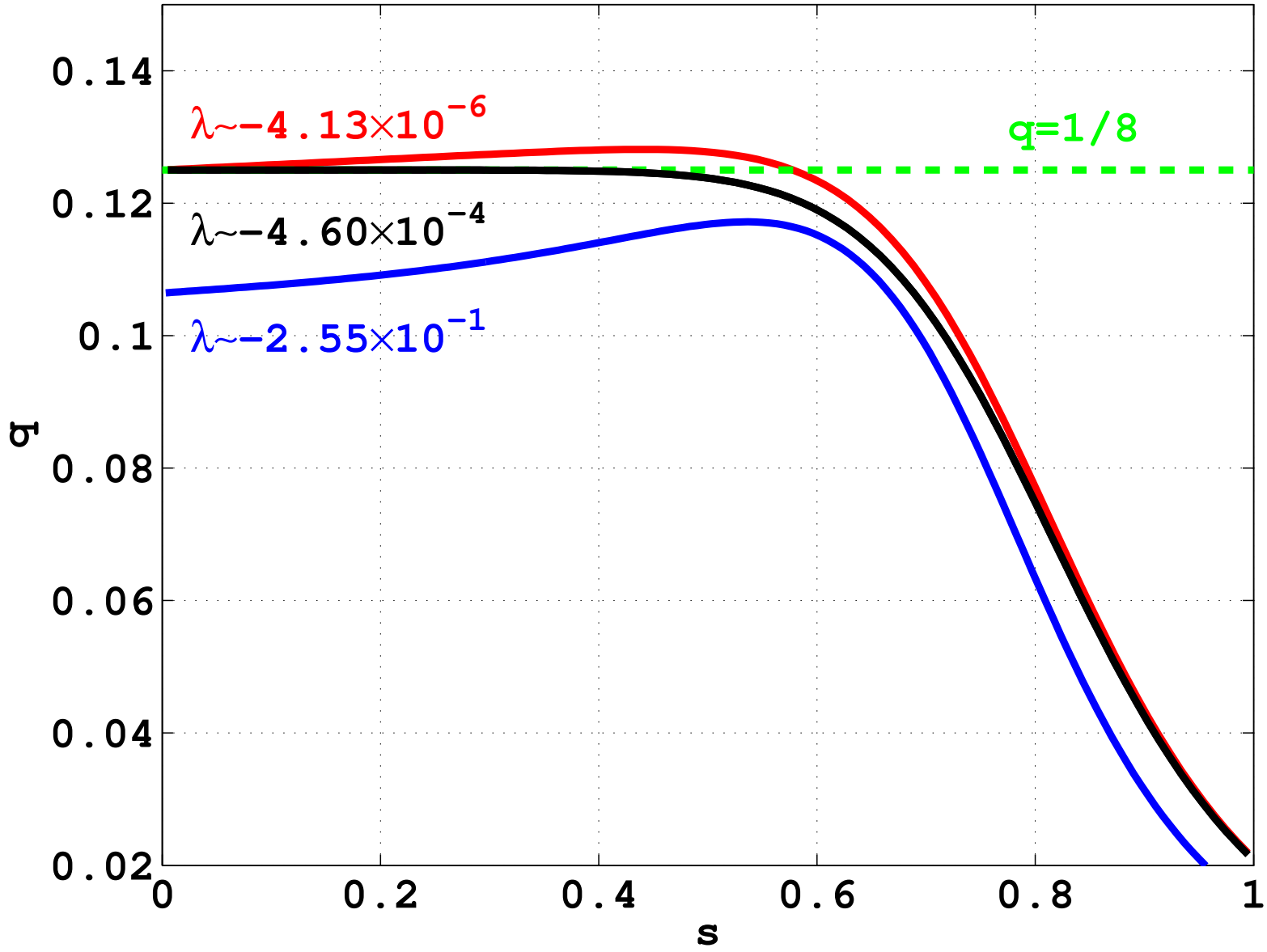

Fourier Amplitudes of ξ^s

- The three leading Fourier amplitudes of the radial component of the displacement vector ξ^s_{mn} with $w/a = 1.198$ and $p = 5$
- for core $q'/q < 0$ for core $q'/q > 0$

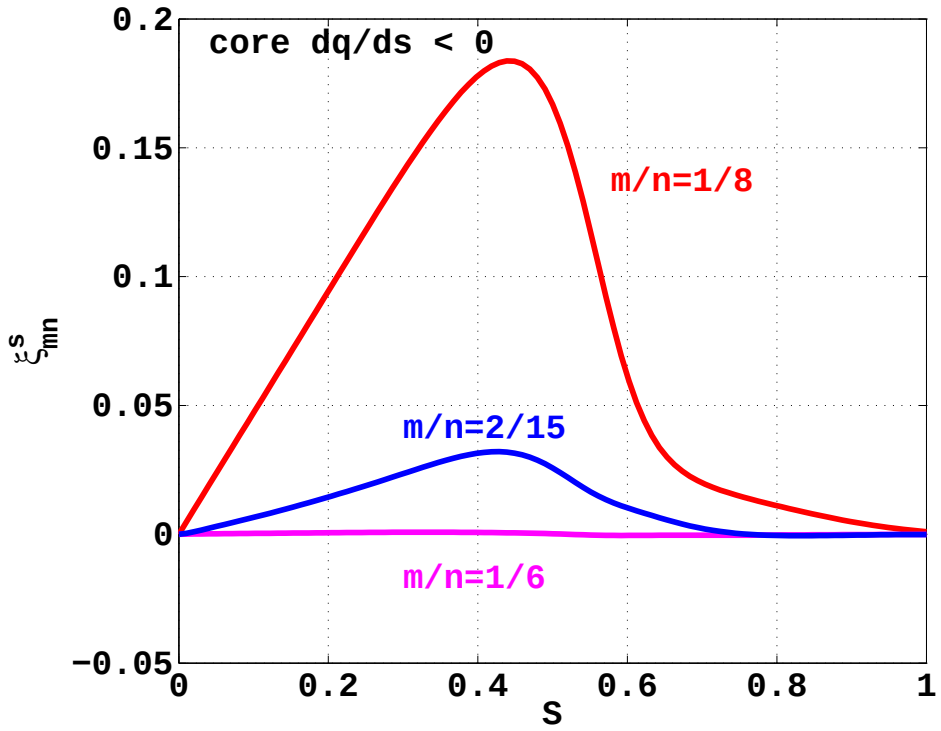

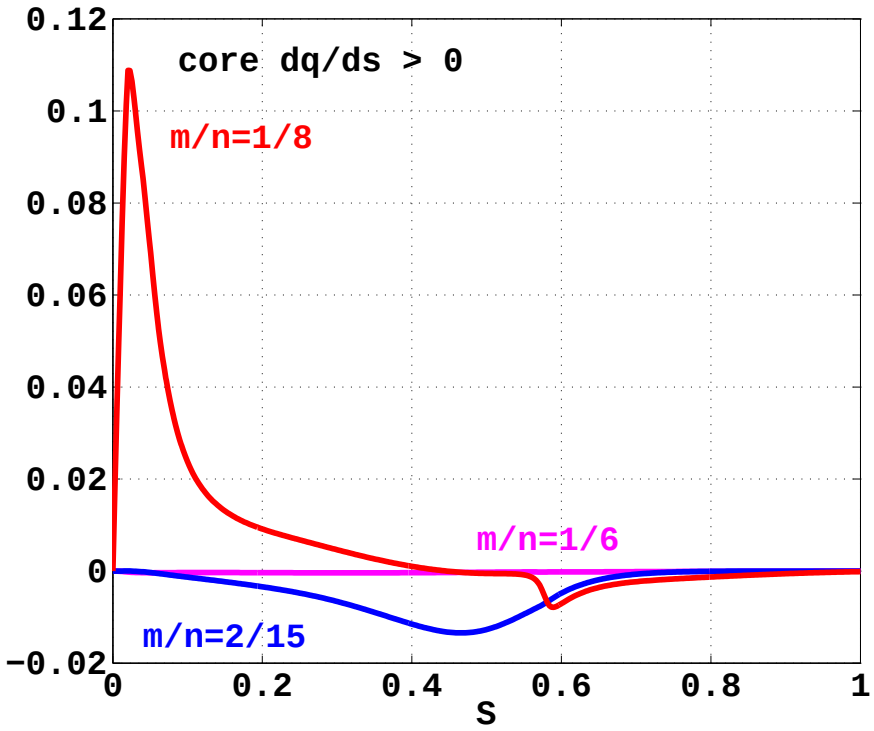

Wall Stabilisation Effects

- λ for core $q'/q < 0$ for core $q'/q > 0$

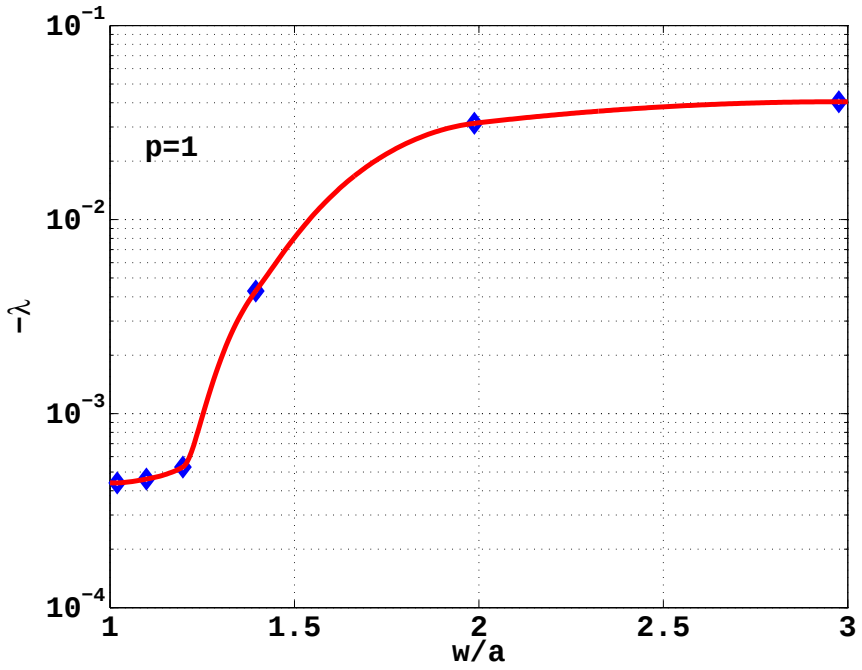

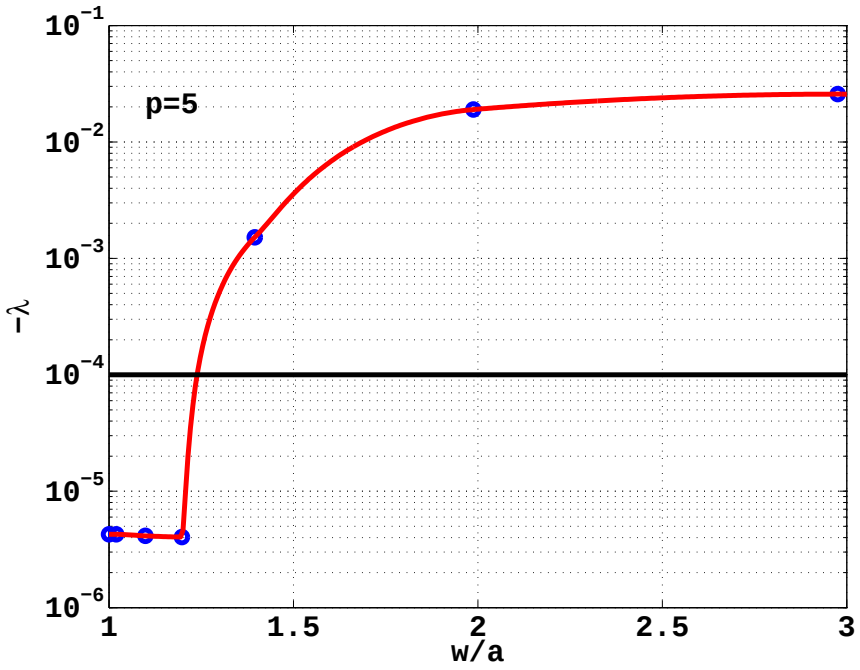

The Instability Driving Terms

- The magnetohydrodynamic instability driving terms correspond to ballooning/interchange (δW_{BI}) and kink (δW_J) structures

$$\delta W_{BI} = -\frac{1}{2}\int_0^1 ds \int_0^{\frac{2\pi}{L_s}} d\phi \int_0^{2\pi} d\theta p'(s)\left[\frac{\sqrt{g}p'(s)+\psi''(s)J(s)-\Phi''(s)I(s)}{B^2} - \frac{\partial\sqrt{g}}{\partial s}\right](\xi^s)^2$$

$$+\int_0^1 ds \int_0^{\frac{2\pi}{L_s}} d\phi \int_0^{2\pi} d\theta p'(s)\frac{B_s}{B^2}\xi^s(\sqrt{g}\boldsymbol{B}\cdot\boldsymbol{\nabla}\xi^s)$$

$$\delta W_J = -\frac{1}{2}\int_0^1 ds \int_0^{\frac{2\pi}{L_s}} d\phi \int_0^{2\pi} d\theta \left[\frac{\sqrt{g}B^2}{|\boldsymbol{\nabla}s|^2}\left(\frac{\boldsymbol{j}\cdot\boldsymbol{B}}{B^2}\right)+\psi'(s)\Phi''(s)-\Phi'(s)\psi''(s)\right] \times\left(\frac{\boldsymbol{j}\cdot\boldsymbol{B}}{B^2}\right)(\xi^s)^2$$

$$-\int_0^1 ds \int_0^{\frac{2\pi}{L_s}} d\phi \int_0^{2\pi} d\theta \left(\frac{\boldsymbol{j}\cdot\boldsymbol{B}}{B^2}\right)h_s\xi^s(\sqrt{g}\boldsymbol{B}\cdot\boldsymbol{\nabla}\xi^s)$$

Perturbed Internal Energy Profiles

- The kink mode driving energy δW_J and the ballooning/interchange driving energy δW_{BI} profiles with core $q'/q > 0$ at different conducting wall positions
- δW_J δW_{BI}

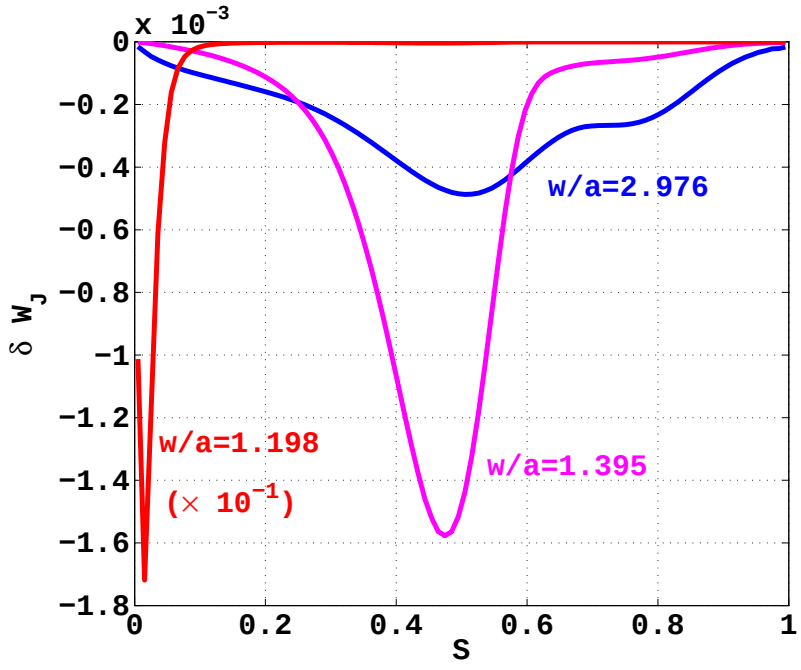

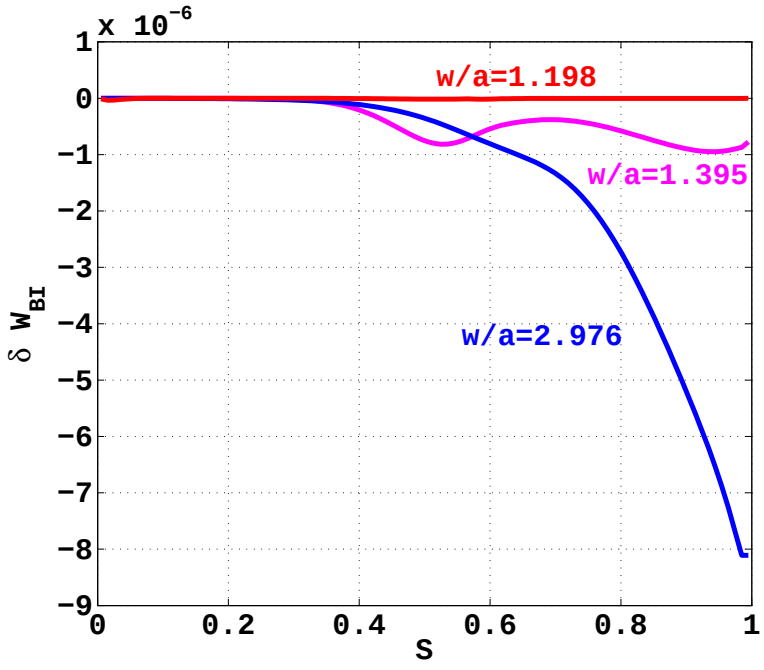

Structure of δW_J

- The structure of the kink driving energy δW_J for core $q'/q < 0$ and $w/a = 2.976$ at three cross sections covering half of a field period ($1/14th$ of the torus)

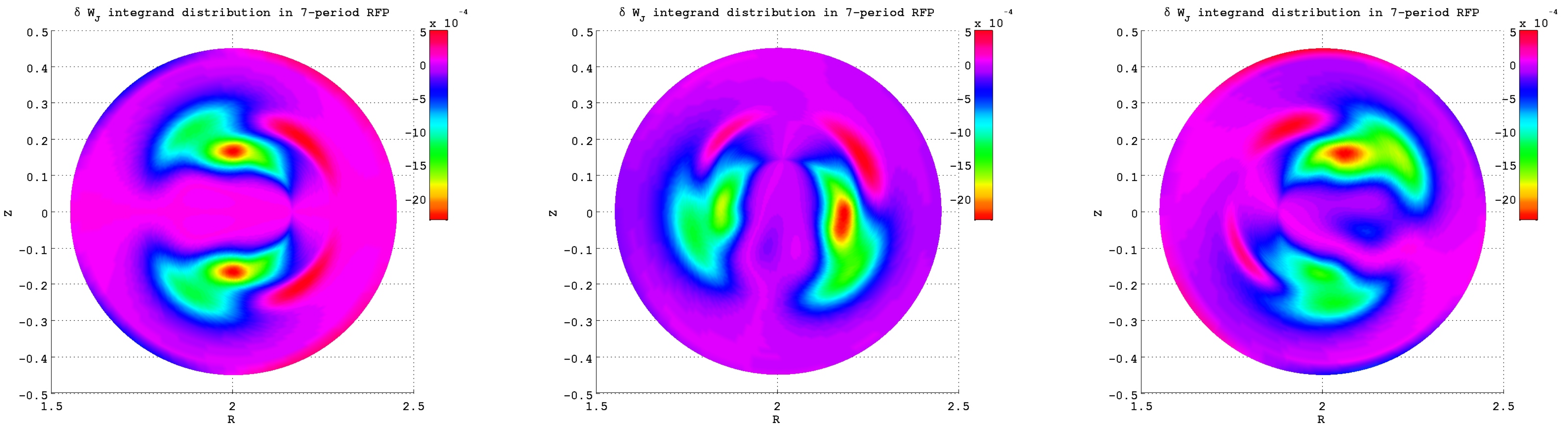

Summary and Conclusions — equilibrium

- Nominally axisymmetric Reversed Field Pinch and Tokamak systems can develop MHD equilibrium bifurcations that lead to the formation of core helical structures.
- In RFX-mod, the development of a SHAx equilibrium state is computed with a seven-fold toroidally periodic structure when q in the core $\sim 1/7$.
- In Tokamak devices, reversed magnetic shear (sometimes just very flat extended low shear) with $q_{min} \sim 1$ can trigger a bifurcated solution with a core helical structure similar to a saturated $m = 1, n = 1$ internal kink.
- We have computed these 3D core helical states in TCV, ITER, MAST and JET. The JET "snake" phenomenon is reproduced with our model.

Summary and Conclusions — MHD stability

- Brief periods in which the relatively quiescent SHAx state in RFX-mod relaxes to a turbulent multiple helicity state are observed —R. Lorenzini et al., Nature Physics **5** (2009) 570 .
- We have investigated the ideal MHD stability of SHAx equilibria by examining mode structures that break the $m = 1, n = 7$ periodicity of the system.
- Either a drop in q well below $1/8$ or the disappearance of core shear reversal triggers ideal MHD modes dominated by $m = 1, n = 8$ coupled with $m = 2, n = 15$ components.
- For $w/a > 1.2$, global unstable kink mode structures are triggered. These kink modes are driven by the Ohmic current. The drive for ballooning and Pfirsch-Schlüter current modes is very weak. The dominant mode structure is a nonresonant $m = 1, n = 6$ component and is basically internal with a finite edge amplitude. Coupling with toroidal sidebands constitutes a significant contribution.

Summary and Conclusions

- In tokamaks, the issue of MHD stability is complicated by the fact that any mode to be investigated is in principle also a component of the equilibrium state. Possible exceptions: local ballooning/Mercier modes, external kink modes, stellarator-symmetry breaking modes.
- The 3D helical core equilibrium states in nominally axisymmetric systems that have been obtained constitute a paradigm shift for which the tools developed for stellarators in MHD stability, kinetic stability, drift orbits, wave propagation or heating, neoclassical transport, gyrokinetics, etc become applicable and necessary to more accurately evaluate magnetic confinement physics phenomena.
- The constraint of nested magnetic flux surfaces and absence of X-points in our model preclude the generation of equilibrium states with magnetic islands. Saturated tearing modes could be investigated with SIESTA, PIES, HINT or SPEC.